THE JOURNAL OF PHYSICAL CHEMISTRY C
A JOURNAL OF THE AMERICAN CHEMICAL SOCIETY

pubs.acs.org/JPCC

Article

Influence of Atmospheric Constituents on Spectral Instability and Defect-Mediated Carrier Recombination in Hybrid Perovskite Nanoplatelets

Published as part of The Journal of Physical Chemistry virtual special issue "D. D. Sarma Festschrift".

Amitrajit Mukherjee, Mrinmoy Roy, Nithin Pathoor, Mohammed Aslam,* and Arindam Chowdhury*

Cite This: https://doi.org/10.1021/acs.jpcc.1c02207

Read Online

ACCESS | Metrics & More | Article Recommendations | Supporting Information

ABSTRACT: Excellent optoelectronic properties make organometallic halide perovskites (OHPs) promising materials for solar photovoltaics and light-emitting devices, however, degradation under various atmospheric conditions severely restricts their potential. To realize stable OHP nanocrystals (NCs) and films resistant to adverse environmental effects, it is imperative to characterize defects created by interactions with surrounding gases and their influence on carrier recombination. Here, we investigate temporal instability of photoluminescence (PL) spectra of individual methylammonium lead bromide ($MAPbBr_3$) nanoplatelets (NPs) under sequential changes of the ambience. In contrast to studies on PL intermittency (blinking) of OHP NCs, spectral trajectories allow us to monitor fluctuations in both PL intensity and transition energy of each NPs in different atmospheres, as well as obtain diversity in nature of active traps under each environmental condition. Analyses of single-NP spectral trajectories in air, Ar, and O_2 under varied moisture contents reveal that exposure to light in dry inert conditions induce deep nonradiative traps in OHP crystals. In contrast, O_2 and moisture mediates efficient radiative recombination via relatively deep and shallow defects, respectively. While the PL features of NPs do switch reversibly between Ar and O_2 (or moist Ar), interaction with moist oxygen under illumination leads to rapid irreversible spectral changes culminating in permanent material degradation. Interestingly, however, removal of moisture from inert (Ar) environments often restores PL spectral features to those observed under dry conditions. This demonstrates that neither oxygen nor moisture individually affects the optical properties of OHP materials as adversely as a combination of the two, which should therefore be avoided to enhance the stability of OHP-based devices.

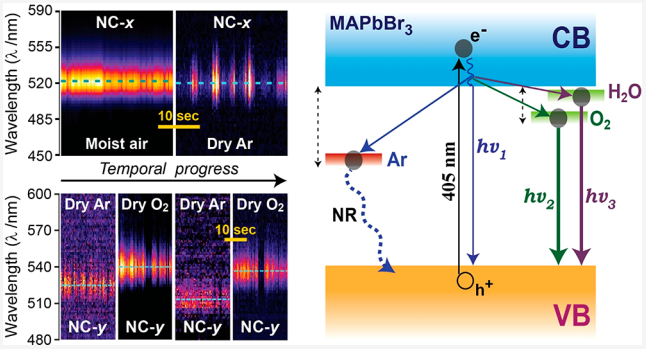

INTRODUCTION

Organometal (hybrid) halide perovskites (OHPs) has attracted significant attention as light harvesting materials for solar photovoltaic (PV)[1,2] and other optoelectronic (OE) applications such as light-emitting diodes (LEDs)[3,4] and tunable lasers[5,6] because of their high absorptivity, photoluminescence (PL) quantum yield (QY) as well as remarkable charge mobility.[7,8] However, photogenerated carrier (electron/hole) trapping in interband defect (trap) states often perturbs charge transportation and initiates nonradiative recombination (NRR) of excitons which adversely affect energy conversion efficiency of PV/OE devices.[9] Importantly, density of such defects increases with environment induced degradation of the "soft" OHPs crystals,[10−22] presumably triggered by trapped charges.[23] Thus, OHP based PSCs or LEDs require delicate control over trap-mediated carrier dynamics in the material, which may be achieved upon understanding the causes for OHP's optical instability under various ambient conditions. This has initiated several studies on the effect of oxygen (O_2) and moisture (H_2O) on photoluminescence characteristics of various OHP materials.[11−19]

Recent reports have revealed that methylammonium (MA) lead halide ($MAPbX_3$, X = Br, I) based thin films (TFs) undergo oxidative photodegradation in the presence of dry oxygen.[11−14] On the contrary, significant PL enhancement in similar OHP microcrystals (MCs) has been observed upon photo-excitation in oxygen atmosphere, which is interpreted as environmental passivation of defects present therein.[24,25] Interestingly, these contrasting observations are explained via

Received: March 11, 2021
Revised: July 13, 2021

interaction of OHPs with the photogenerated superoxides under moisture-free O_2 atmosphere, which can either increase[12,13] or passivate[24−28] the trap (defect) states. Moisture (H_2O) in the surroundings also severely affects the optical and electronic properties of OHPs, and prolonged exposure to high relative humidity (RH) is known to permanently degrade perovskite materials.[10,11,19−22] In contrast, limited exposure to moisture can passivate surface traps which enhances the photoemission.[26,28,29] Intriguingly, exposure to higher relative humidity (RH ∼ 85−90%) does not always completely degrade OHP crystals; for $MAPbBr_3$ films, a significant proportion of PL intensity (I_{PL}) reappears after lowering the RH to 15−20%.[30] Such reversibility of optoelectronic behaviors likely owes to dynamic adsorption/desorption of moisture at the surface of OHP lattice.[10,11] Further, initial PL enhancement of OHP-TFs and subsequent gradual decline upon prolonged illumination has been explained via initial light and O_2/H_2O-induced trap-passivation, which is surpassed at longer times by parallel NR trap-generation due to material degradation.[31,32] However, it is still unclear whether O_2/H_2O independently interacts in multiple ways to create or remove crystal defects and how a combination of these two atmospheric constituents affects the photophysical properties of OHP materials. Such information provides insight on atmosphere induced degradation of OHPs and thus, it is crucial to investigate the nature of active photoinduced traps under specific environmental conditions.

In this context, probing PL intermittency ("blinking") of OHP nanocrystals (NCs),[33−35] microcrystalline rods,[36,37] and films[34,38−40] becomes relevant to study the nature of defect states under different environments.[14] While PL intermittency for OHP NCs has been related to surface defects involved in carrier recombination pathways,[14,33−35] similar to that for conventional inorganic NCs,[41] blinking/flickering of microcrystalline disks/thin-films[36,38,39] is attributed to transient mobile defects which act as strong quenchers.[36,40] More importantly, different blinking characteristic as well as gradual change in PL intensity over slower time scales (second to minute) has been ascribed to generation or passivation of various (deep/shallow) trap states during degradation or curing of the material in the presence of light[9,42−44] and atmospheric conditions.[10,14,30,33,35] Thereby, nature of the defects involved in the emission cycle have often been related to the emissivity of the crystals.[14,33,34,45−47] However, PL intermittency and emissivity of OHP NCs from different systems are found to be contrasting under the similar atmospheric conditions suggesting the different nature of active defects.[14,33] Moreover, like inorganic quantum dots,[48] OHP NCs of similar composition and morphology can also exhibit heterogeneous blinking characteristics in the ensemble under identical measurement conditions which likely owes to diverse origin and distribution of defects in the crystals.[49,50] Therefore, it is necessary to investigate the same NC as well as the large population of individual OHP crystals under sequential environments in order to reliably correlate their PL characteristics, which has rarely been attempted.[33]

In addition to intermittency, PL spectroscopy and lifetime measurements have been performed to probe the nature of traps involved in OHP NCs[45−47] or TFs[29,51−53] under the influence of oxygen or moisture.[29] Previous studies show that moisture can deactivate shallow defects in $MAPbX_3$ (X = Br, I) TFs,[10,29] while calculations suggest that oxygen can passivate deep traps.[27] Further, spectroscopic and/or lifetime data on OHP NCs/TFs[45−47,10,29,42,51−54] have revealed that environmental/chemical passivation of NR defects, or the creation of radiative traps in defect rich grains,[10,55] can lead to intense emission Stokes shifted from the band-edge. Interestingly, spectral diffusion of single OHP NCs suggest the existence of radiative traps in aerial environments, however, there is variation among NCs on the extent of defect-induced spectral shifts.[56] Moreover, emission spectra of individual NCs of all-inorganic perovskites ($CsPbX_3$; X = Br, I) have shown several interesting phenomena, such as continuous, irreversible blue shift in transition energies (E_{PL}) because of photo-oxidation of NCs under ambient conditions.[46,47] Therefore, to obtain clues on activation/deactivation processes and nature as well as energetics of defects, a systematic investigation is warranted on the PL spectral characteristics of individual OHP NCs upon change in the surrounding environment, which may additionally allow evaluation of (ir)reversible material degradation.[47]

In this work, we investigate environment dependent PL intermittency and spectral characteristics of individual $MAPbBr_3$ nanoplatelets (NPs) which have been recently demonstrated to exhibit superior crystallinity, reduced NR dynamics, higher exciton binding energy, and carrier mobility, especially desirable in active layers for PV/OE applications.[57−59] Here, we performed PL spectroscopic measurements on same layered NPs under sequential (and reversible) changes in different atmospheric constituents such as air, O_2, and argon (Ar). Further, we investigated the effect of humidity (H_2O) on both blinking and transition energies under each environmental condition. Importantly, to avoid complicacies in inference because of heterogeneity in emission properties,[48] we studied a large number of individual NPs which allowed us to understand the nonuniformity in emission processes as well as probe how the majority intermittency/spectral characteristic of the ensemble changes with varied atmospheric conditions. On the basis of our single-particle PL spectral measurement and existing literature data, we propose a viable mechanism for atmosphere-induced carrier recombination and material instability of layered $MAPbBr_3$ NPs.

MATERIALS AND METHODS

Synthesis of $MAPbBr_3$ Nanoplatelets. Dodecylamine-oleic acid capped single $MAPbBr_3$ nanoplatelets (∼50−60 nm edge length) were prepared following a previously developed procedure by Roy et al.[60] In brief, $PbBr_2$ (0.18 mmol) was loaded into a 100 mL three-neck round-bottom flask with 5 mL of 1-octadecene (ODE) and heated to 120 °C with continuous stirring under N_2 atmosphere. $PbBr_2$ becomes completely dissolved by the addition of oleic acid (OA, 0.7 mL) and dodecylamine (0.3 mL) under continuous N_2 flow. The temperature of the reaction mixture was maintained at 120 °C with continuous stirring for 1 h, which further decreased to 60 °C followed by the rapid addition of 0.17 mL methylamine (MA) solution (2 M) in tetrahydrofuran along with 0.7 mL of OA, which yielded instantaneous formation of the $MAPbBr_3$ NPs. The perovskite NPs were separated by centrifugation for 10 min at 8000 rpm and dried in the desiccator.

Characterization. X-ray diffraction (XRD) of $MAPbBr_3$ NPs was performed using an Xpert PANAlytic X-ray diffractometer with Cu Kα radiation (λ = 1.5406 Å) with an operating voltage and current of 40 kV and 30 mA, respectively. The XRD pattern (Figure S1a) indicates the pure cubic phase of $MAPbBr_3$ NPs with space group $Pm\bar{3}m$

https://doi.org/10.1021/acs.jpcc.1c02207
J. Phys. Chem. C XXXX, XXX, XXX−XXX

(JCPDS 252415). Calculated lattice parameters of the crystals are a = 5.97 Å, b = 5.92 Å, c = 6.03 Å. The morphological study of the NPs has been performed using a field emission gun transmission electron microscope (FEG-TEM) and selected area electron diffraction patterns (SAED) obtained with JEOL JEM 2100F instrument at an accelerating voltage of 200 kV. This reveals layered type of structure of $MAPbBr_3$ NPs (Figure S1b) having 50 to 60 nm edge to edge length, analogous to Ruddlesden−Popper phase which consists of 2D perovskite-like slabs interleaved with cations. General formula for this kind of perovskite is $(R{-}NH_3)_2(CH_3NH_3)_{n-1}Pb_nBr_{3n+1}$, where R is dodecylammonium cations and n is the number of continuous octahedra which are stacked together in the perovskite structure, for example, in our case $n \geq 5$. The set of rings in the SAED pattern (inset, Figure S1b), corresponding to the (300), (210), and (200) planes of $MAPbBr_3$, confirms polycrystalline nature of the NPs. Bulk absorption spectra of $MAPbBr_3$ NPs suspended in dry toluene was acquired using PerkinElmer Lambda 950 UV−vis spectrometer, which shows the absorption peak at 526 nm (Figure S1c). We calculate the bandgap of bulk NPs at 2.2 eV (Figure S1d) from the absorption spectra using Tauc's method.[61] Ensemble photoluminescence (PL) measurement of the bulk $MAPbBr_3$ NPs is performed using Horiba Fluoromax 4 instrument with 440 nm excitation with 2 nm slit width. PL measurement shows a sharp emission peak at 528 nm (~2.35 eV) and ~95 meV full width at half maxima of the emission spectra (Figure S1c). The emission quantum yield of the $MAPbBr_3$ NPs investigated here has been evaluated to be ~0.4.[60]

Single-Particle PL Spectroscopy. Thin film of $MAPbBr_3$ NPs was prepared via spin coating (2000 rpm for 1 min) a dilute (~nM) solution in dry toluene (spectroscopic grade, Sigma-Aldrich), on a freshly cleaned glass coverslip (25 mm × 25 mm). The wide-field epifluorescence microscopy of spatially segregated NPs was performed by exciting a large area (~40 μm diameter) of the TF with 405 nm continuous wave (cw) laser (100 μW, power density ~8 W cm^{-2}) using an oil immersion objective lens (1.49 NA, 60×, Nikon ApoTIRF, oil). The PL from the single NPs were passed through the same objective lens followed by 457 nm long-pass dichroic filter and detected using an interline CMOS camera (Hamamatsu orca flash 4.0 v3). Single NPs spectroscopy was performed by placing a variable, vertical slit in the emission pathway for spatial selection of emitters, accompanied by a transmission grating (70 grooves/mm). The detailed description of the experimental setup can be found elsewhere.[62] Blinking movies (16 bit images) are collected at 100 Hz while single emitter spectroscopy is performed at 10 Hz (frames/sec) acquisition rate. Because of the instrumental limitations for long time data collection, we acquired 100 s data which is consistent for all samples. Each movie containing few tens of single emitters is analyzed after background flattening using *ImageJ* software. PL intermittency and spectroscopy of individual $MAPbBr_3$ NPs were performed under varying local environments such as Argon (Ar) and O_2 in both dry and carefully monitored humid conditions in addition to moist (RH ~ 55%) ambient environment (Air). A glass chamber with humidity sensor, containing an inlet and outlet, was attached to the microscope stage to attain desired local atmosphere. Dry gases (Ar or O_2) were purged into the chamber through the inlet either directly or through water to achieve dry or humid environment. Each of the corresponding dry gases were purged for 30 min before measurements, without exposing the NPs to light. All data were collected at 295 K. Single NP emission spectra are fitted with single Gaussian function to obtain relevant spectral parameters.

RESULTS AND DISCUSSION

Optical Instability Characteristics of OHP NPs under Various Environments. Because of extremely high PL intensity observed in the ensemble emission spectra (Figure S1c), spatially segregated layered NPs of $MAPbBr_3$ could be readily imaged with high contrast (Figure 1a, inset), although

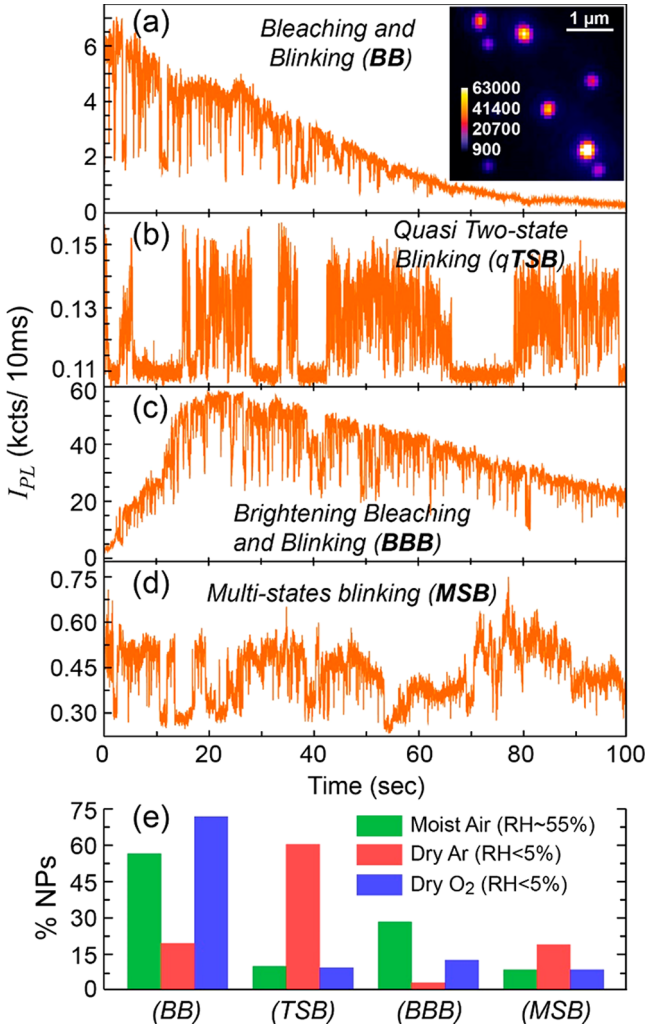

Figure 1. (a−d) Diverse PL intermittency and emissivity characteristics of various individual $MAPbBr_3$ NPs (1a, inset) under identical experimental conditions: (a) BB, (b) qTSB, (c) BBB, and (d) MSB. (e) Relative frequency of PL intermittency characteristics (a−d) under three different environments. The number of $MAPbBr_3$ NPs' PL intensity trajectories investigated: 221 (moist air), 504 (dry Ar), and 604 (dry O_2).

there is considerable heterogeneity in the brightness of different NPs (Figure 1a,b). Subsequently, we collected emission (movies) over 100 s duration for many individual $MAPbBr_3$ NPs under different ambient conditions, which allowed us to compare the rudimentary differences of optical instability features in moist air, dry O_2, and dry Ar. We find that the NPs undergo significant temporal fluctuations of emissivity in terms of (i) gradual changes in emission intensity such as photobleaching or photobrightening and/or (ii) abrupt

https://doi.org/10.1021/acs.jpcc.1c02207
J. Phys. Chem. C XXXX, XXX, XXX−XXX

blinking or flickering between two ("On"/bright and "Off"/dark) or more intensity levels, apart from (iii) wide variation in the maximum PL intensity over a course of time. Several characteristic of PL intensity trajectories under ambient conditions (air) are shown in Figure 1a−d. As opposed to the prior reports,[14,33] our data clearly reveal that the nature of PL fluctuations as well as emission yields vary considerably for different individual NPs in the ensemble under a specific environmental condition. On the basis of these aspects, we classified the blinking propensity of single NPs into four dominant categories (Figure 1a−d), namely (i) "Bleaching with blinking" (BB) (high initial intensity), (ii) "Quasi two-state blinking" (qTSB) (low to moderate intensity; emissivity of this class of NCs with higher occurrence of the long Off-intervals (On-intervals) are designated "Mostly Off" ("Mostly On") type emitters), (iii) "Photobrightening and bleaching with blinking" (BBB) (moderate to high intensity, also see Figure S2a), and (iv) "Multistate blinking" (MSB) (low to moderate intensity). Although not discussed further, it is worth mentioning that we identified few rare events (∼2%) of bright NPs only under dry O_2 environments which show continuous photobrightening accompanied by blinking (Figure S2b).

Our measurements on several hundreds of $MAPbBr_3$ NPs show that these four optical instability characteristics are ubiquitous irrespective of all the environments studied. However, their relative proportions and dominant behaviors change remarkably when the environmental constituents in the surroundings are altered (Figure 1e and Table S1). Out of 221 NPs investigated in (moist) air, an overwhelming majority of emitters exhibit either BB (∼57%) or BBB (∼28%) type blinking (Figure 1a,c) and seldom do we find qTSB or MSB intermittency. However, in subsequent inert atmosphere (dry Ar), we find significant lowering of PL intensity for the vast majority of NPs, and the dominance (60%) of qTSB (Figure 1b) along with a smaller proportion (∼20%) of MSB (Figure 1d) behaviors. On the other hand, in dry O_2 environment (after Ar) there is a considerable enhancement of the initial emission intensity for most of the NPs (∼75% of 605 emitters), which undergo slow time scale photobleaching accompanied by blinking (BB). However, nearly a quarter of total NPs investigated in dry O_2 do exhibit diverse intermittency behaviors (qTSB, BBB, and MSB) in almost equal proportions.

The contrasting behaviors (i.e., dominant qTSB or BB) for most NPs (Table S1) in the absence and presence of inert (argon) environment (qTSB) suggests that slow temporal decay of PL along with abrupt intermittency with short Off-time durations, is a consequence of interactions of the crystals with oxygen. Further, in moist air/dry O_2, we often observe the feature of either abrupt or gradual enhancement of PL intensity (BBB) up to a critical time (τ_c) followed by a decay in PL, in which τ_c varies from milliseconds to several tens of seconds for different NPs. Thus, surrounding O_2 and/or H_2O can cause passivation of certain nonradiative (NR) defects leading to initial PL enhancement, however, a competing process of activation of other NR traps due to environmental degradation or photoexcitation is simultaneously operational and becomes dominant after τ_c. We note that such initial enhancement and subsequent diminishing of PL emissivity has been observed in nonblinking bulk OHP crystals and films as well.[31,32]

While the exact reason remains unclear, the large variation of τ_c from one NP to the other may be related to the initial density of defects (or traps) present in each crystal prior to the photoexcitation, which can severely affect oxygen or moisture induced trap-passivation or activation processes. Further, increase in proportions of BB type intermittency in dry O_2 atmosphere (Table S1) with respect to moist air (RH ∼ 55%) indicates that higher vapor pressure of oxygen assists in degradation of the NPs from the initial exposure of light. This inference is supported by lower density of emitters found under dry O_2 environments, following initial measurements in moist air and argon (Figure S3). It is also relevant to note that the majority of $MAPbBr_3$ NPs are considerably more photostable in the presence of dry Ar due to lack of involvement of oxygen/moisture in assisting photodegradation. However, there is a significant lowering of the emission intensity along with rarely emissive qTSB (Mostly Off) characteristics under inert condition, consistent with prior reports.[28,33,42,63] This behavior likely owes to activation of deep traps under photoirradiation, which enhances alternate NR recombination channels thereby significantly lowering the emissivity.

It is relevant to note that the NPs are encapsulated by organic ligands (dodecylamine), which form the first point of interaction of gaseous molecules. It is possible, however, that the density and/or distribution of ligands around various $MAPbBr_3$ NPs are quite diverse, and therefore the effective barrier faced by gas molecules surrounding the NPs can vary. We speculate that local uncovered (or sparsely covered) surface of NPs may act as interaction zones with gases, and these regions can generate/passivate specific traps which influence optical properties. Thus, the density or the nature of defects/traps that are formed/removed by an atmospheric constituent is likely to differ from one NP to another, which may result in a wide variety of blinking characteristics observed in our measurements.

While the above measurements provide an overall idea about the emissive behaviors of $MAPbBr_3$ NPs in diverse environmental conditions, issues such as reversibility cannot be deciphered conclusively. Further, because of significantly reduced emission spots in moderate to high humidity, it is challenging to perform statistical analysis of PL intermittency upon progressive change of the environmental moisture content. Therefore, it is imperative to monitor the PL intermittency and emissivity characteristics of individual NPs upon sequential change of surrounding atmospheric constituents, which provides insights into role of oxygen and moisture on each OHP particle's optical instability.

Effect of Environmental Constituents on PL Intermittency of Individual OHP NPs. We use three representative NPs (NP-1 to NP-3) which have similar initial PL intensity and comparable intermittency characteristics in air, to portray the effect of atmospheric constituents on PL characteristics. First, we investigated sequentially collected PL intermittency of NP-1 (Figure 2a) under humid air, followed by exposure to dry Ar, and eventually under dry oxygen atmosphere. Consistent with our previous observations (Figure 1e and Figure S3, Table S1), we find that the emissivity of NP-1 is remarkably decreased in inert environment (qTSB) as compared to moist air (BB), while high PL intensity is restored under subsequent exposure to dry O_2 (Figure 2a, Figure S4a). Further, under Ar, blinking involves predominantly Off-states with intermittent short-duration On bursts, which is in stark contrast to aerobic environment where the emitters remain mostly in the On or bright state. This particular NP, like most others in the ensemble, was also found to undergo a complete

https://doi.org/10.1021/acs.jpcc.1c02207
J. Phys. Chem. C XXXX, XXX, XXX−XXX

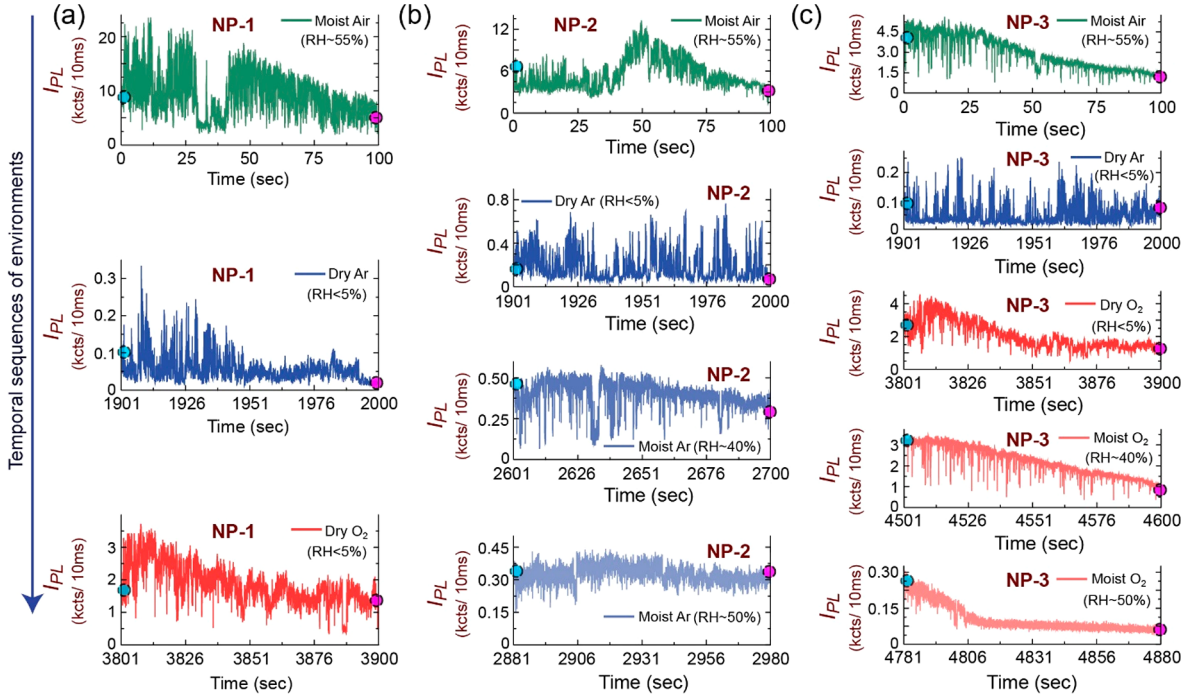

Figure 2. (a) PL intensity trajectories of NP-1 under moist air (green), followed by dry Ar (blue), and dry O_2 (red). (b) PL intensity trajectories of NP-2 in air (green), followed by dry Ar (blue), and moist Ar. (c) PL intensity trajectories of NP-3 in air (green), followed by dry Ar (blue), neat O_2 (red), and moist O_2. Individual NPs undergo irreversible degradation under high humidity (RH > 50%) which is further augmented in the presence of oxygen. Traces collected in moisture environments are shown using lighter shade.

loss of emissivity upon further exposure to dry Ar (and dry O_2), which suggests irreversible material degradation in the presence of high vapor pressure of O_2 in combination with light exposure. Moreover, to investigate whether light-induced trap-filling (in air) affects the emissivity, we monitored the PL of NPs under alternating dry Ar and dry O_2 environments without prior illumination under ambience. We found that intermittency characteristics of NPs is identical (Figure S5i,ii) in the respective environments (dry Ar or O_2) which implies that atmospheric influence dominates significantly over photoinduced trap-filling processes.

To probe the role of moisture, we investigated PL intermittency of individual NPs under inert and varied humid atmospheres, in the sequence Air−Ar(dry)−Ar(RH ∼40−50%)−Ar(dry), shown using the representative $MAPbBr_3$ NP-2 (Figure 2b, Figure S4b). In agreement with previous results, NP-2 undergoes BBB characteristic in moist air while intermittency subsequently changes to qTSB with much lower intensity under dry Ar (Figure 2b, Figure S4b). Further, we find that moderate humidity (RH ∼ 40%) enhances the average PL intensity of NP-2 for up to ∼36 s (τ_c), which gradually decays over long time while undergoing frequent blinking (BBB). With increasing moisture in Ar, there is a progressive decrease of the maximum intensity up to RH of ∼50% where blinking ceases to occur and the emission stabilizes. It is relevant to note that, in contrast to dry Ar, moisture (in Ar) typically transforms NPs to Mostly On type emissivity (Figure 2b). Moreover, we noticed that similar to NP-2, most of the NPs irreversibly bleaches (Figure S6) at higher moisture level (≥RH ∼ 60%) and does not reappear even upon reversing to dry Ar environments. Therefore, while low amount of moisture can passivate certain NR traps in oxygen-free (inert) environments, there is complete and irreversible degradation of vast majority of $MAPbBr_3$ NPs at higher moisture levels.

Next, we probed the influence of varied amounts of moisture in oxygen, on the PL characteristics of individual $MAPbBr_3$NPs. Figure 2c depicts intermittency characteristics of NP-3 with increasing moisture content (RH ∼ 5−50%) in oxygen subsequent to initial exposure to air and dry Ar. NP-3 also follows the same trend (BB → qTSB → BBB) as in NP-1 (Figure 2a) under sequential exposure to Air, dry Ar, and dry O_2 (Figure 2c). At RH of ∼40% NP-3 undergoes blinking along with bleaching similar to that observed for NP-2 in moist Ar (Figure 2b, RH 40%), however, there is a clear enhancement in photobleaching rate in the presence of dry oxygen. Further increase of the RH to ∼50% significantly lowers the initial emission intensity (Figure 2c, Figure S4c) and rapidly photodegrades the emitter. We subsequently exposed the same NP-3 to even higher moisture (RH ∼ 60%), where the emitter remained nonemissive, similar to the behaviors of overwhelming majority of NPs in the ensemble. Upon reversal to dry O_2 or inert (Ar) environments, most of these NPs (which have been exposed to high humidity and oxygen) do not show any enhancement of PL emission, indicating irreversible degradation of the crystals. Therefore, exposure to higher moisture in any environment is more likely to irreversibly and adversely affect the optical property of $MAPbBr_3$ NPs. Although their effects are similar, we refrain from concluding that either oxygen or moisture is more detrimental toward $MAPbBr_3$ NPs, as their extent of degradation can be rather diverse in both of these environments and likely depends on the initial defect density in each NP (Figures S6 and S7).

Importantly, under dry O_2 and/or moisture, individual NPs exhibits almost 10-fold increase in the (initial) PL intensity as compared to prior exposure to (dry) Ar, however, their

https://doi.org/10.1021/acs.jpcc.1c02207
J. Phys. Chem. C XXXX, XXX, XXX−XXX

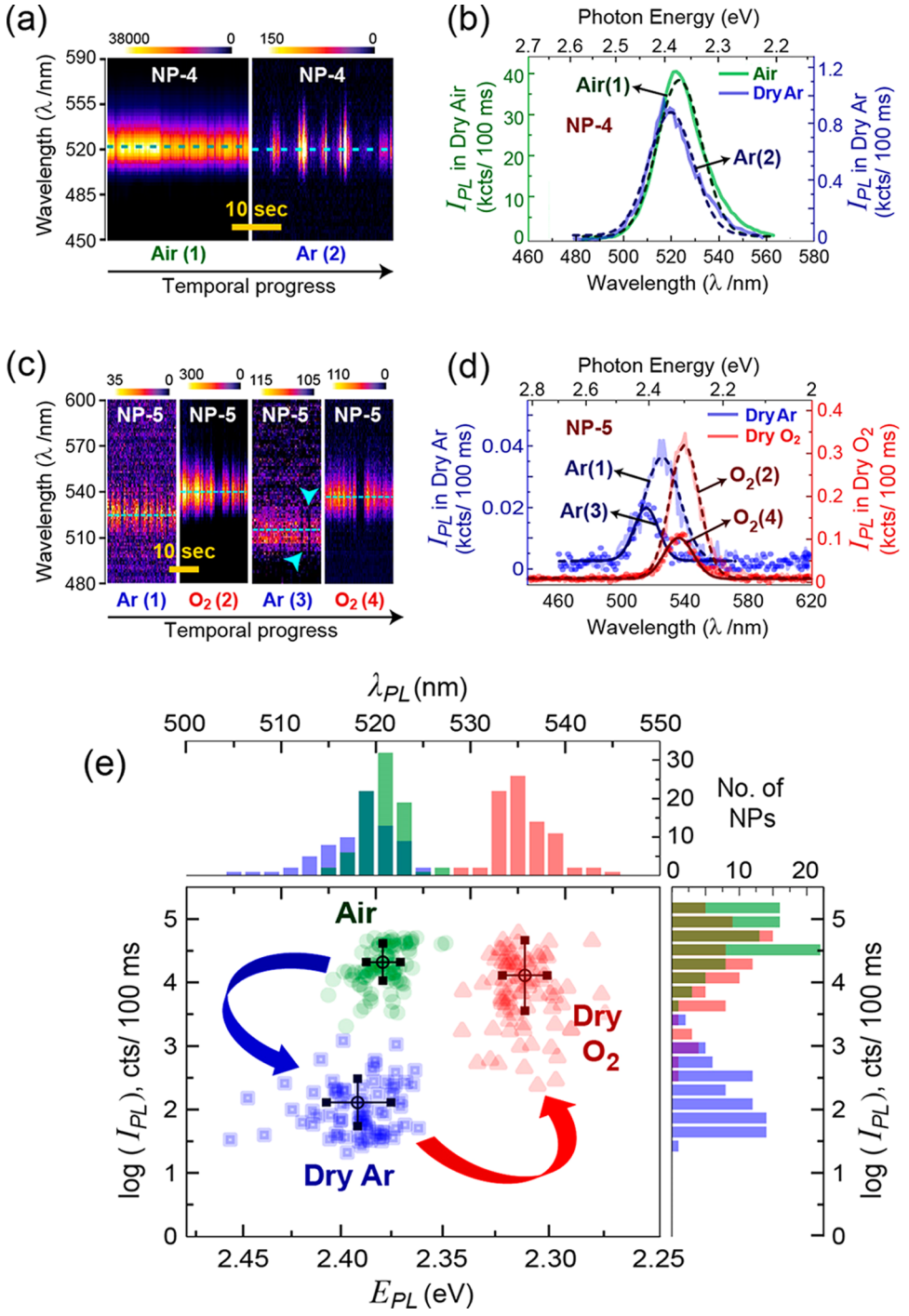

Figure 3. (a) PL spectral trajectories of NP-4 under Air followed by Ar and (b) the corresponding time averaged emission spectra in the two environments. (c) Spectral trajectories of NP-5 in Ar followed by O_2, Ar, and O_2 environments, and (d) the corresponding sequential changes in the time averaged emission spectra. (e) Bivariate plot and frequency distributions of E_{PL} and I_{PL} constructed from the spectral analyses of 80 $MAPbBr_3$ NPs in sequentially varied environmental conditions (Air, green circles; Ar, blue squares; O_2, red triangles). The mean values and standard deviations of E_{PL} and I_{PL} in each environment are depicted using circles and line segments, respectively.

intermittency characteristics switch from being Mostly Off to Mostly On (Figures S6 and S7). This suggests both water and oxygen molecules in the environments affect the emission process of NPs in a similar fashion, often involving simultaneous passivation and activation of certain traps. Further, it is relevant to mention that the influence of moisture is more dramatic (within few minutes) in comparison to dry oxygen, where longer exposure is required to observe the same effects. However, it is still unclear whether oxygen and water interaction is selective toward similar nature (deep/shallow) of the defect states. So, to unravel or infer on the energetics of involved defects, we next investigated how emission spectra from individual NPs are altered under specific and sequential atmospheric conditions.

Spectral Instability of Individual OHP NPs under Varying Environmental Conditions. While blinking indicates active trap mediated NR recombination channels, it does not provide information on energetics of the emissive

https://doi.org/10.1021/acs.jpcc.1c02207
J. Phys. Chem. C XXXX, XXX, XXX−XXX

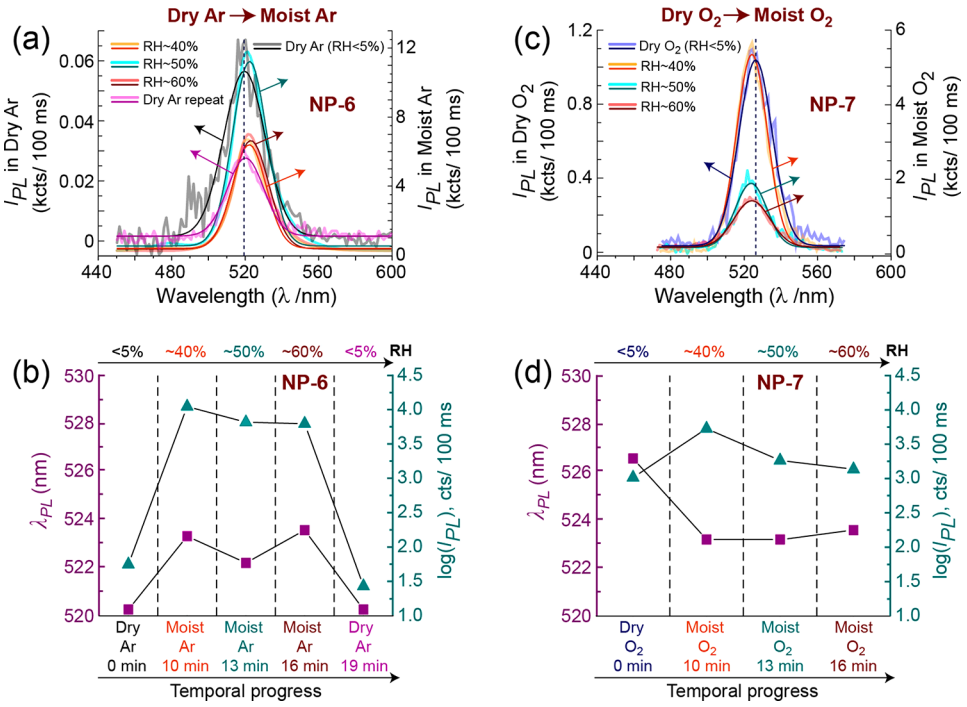

Figure 4. (a) PL emission spectra of NP-6 under Ar environments with increasing moisture (sequence: RH of 5%, 40%, 50%, 60% and 5%) along with Gaussian fits from which I_{PL} and λ_{PL} were extracted. (b) The corresponding change in λ_{PL} (squares) and I_{PL} (triangle) of NP-6 between dry and moist Ar. (c) PL emission spectra of NP-7 under O_2 environments with increasing moisture (sequence: RH of 5%, 40%, 50%, and 60%) along with Gaussian fits from which I_{PL} and λ_{PL} were extracted. (d) The corresponding change in λ_{PL} (squares) and I_{PL} (triangles) of NP-7 between dry and moist O_2. Initially, none of the NPs were exposed to light in air and the time points of measurements are depicted in (c,d). Vertical dotted lines (black) in (a,c) represents initial λ_{PL} positions.

states, and how it varies in the presence of different environmental constituents. Here, we investigate the PL spectra as a function of time for individual $MAPbBr_3$ emitters (NP-4) under Air−Ar(dry) atmospheric sequence. The spectral time-trajectory of one such typical emitter (NP-4) is depicted in Figure 3a, which undergoes qTSB under dry Ar. The corresponding time-averaged emission profile of NP-4 along with single-Gaussian fits (Figure 3b) reveal a slight blue shift of transition energy (~15 meV) in Ar along with an ~4-fold lowering of intensity as compared to humid air (also see Figure S8a,b).

Next, we monitored the effect of (moisture-free) O_2 and Ar on the emission spectral dynamics of individual NPs under alternating sequence of these gases without prior exposure to light (in air). Figure 3c shows the changes in spectral trajectories for an OHP crystal (NP-5) upon switching back and forth between Ar and O_2 surroundings. For NP-5, the time-averaged PL spectra exhibit prominent yet reversible change in both emission intensity (~8−10 times) and transition energies (Figure 3d), and the extent of energetic changes can be as high as ~135 meV (Figure S8c,d). We note that after O_2 purge, most single NPs become so weakly emissive that it is challenging to detect these on further exposure to Ar. However, upon reintroduction of O_2 environment, NPs exhibit significantly enhanced PL (compared to Ar) and their spectral peaks revert back close to their respective positions in O_2 (Figure 3c,d and Figure S8c,d). This suggests that while the NPs are not completely degraded, more NR defects are created upon progressive exposure to oxygen. Intriguingly, for the few NPs (such as NP-5) from which emission spectra could be collected during second exposure to Ar (after O_2), the PL peak positions (λ_{PL}) are often found to undergo significant blue shift compared to that observed initially in Ar (Figure 3c,d). While the exact reason remains unclear, such spectral bluing can arise from partial degradation of the $MAPbBr_3$ NPs upon interim exposure to oxygen and light.[46,47,64]

To obtain time-averaged behaviors of a larger population of NPs, we collected the emission spectra of random particles under each of the aforesaid conditions. Subsequent emission spectral analyses of ~80 such NPs in each environment yielded distributions of parameters such as transition energies, emission intensities and line widths (Figure 3e and Figures S9 and S10). The effect of the environmental constituents on the mean values of PL peak positions (Figure 3e) is consistent with that observed for individual NCs (Figure 3a,c); there is a slight blue shift (~15 meV) from air (2.38 eV) to Ar (2.394 eV), however, the average E_{PL} undergoes dramatic red shift (~80 meV) from Ar to dry O_2 (2.313 eV). The bivariate plot of intensity maxima against transition energy for all these NPs (Figure 3e) reveals a significant reduction in the emission yield in inert environment, consistent with our blinking data (Figure 2). Relatively low spectral blue shifts upon introduction of Ar suggest that in air, carriers can recombine via shallow radiative traps, which are not accessible under inert environments. It is reported that photoinduced deep NR traps can be formed under inert (N_2) surroundings[28,33,42,63] or evacuated conditions[28,31] and are likely to be responsible for significant quenching of PL in argon. The reversible and prominent emission enhancement and red shift (Figure 3c,d, Figure S8) further suggests that dry O_2 can passivate NR traps formed in Ar,[27] thereby initiating radiative recombination (RR) processes from relatively deeper trap levels. In addition, upon switching from moist air to dry oxygen (Figure S11) results in a nominal

https://doi.org/10.1021/acs.jpcc.1c02207
J. Phys. Chem. C XXXX, XXX, XXX−XXX

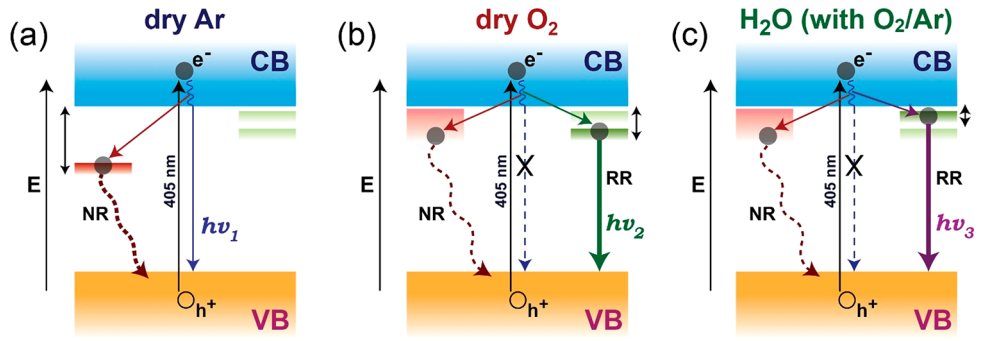

Figure 5. Schematic depiction of proposed carrier recombination pathways in $MAPbBr_3$ NPs under (a) Ar, (b) O_2, and (c) moist O_2 or Ar. Dashed curly and straight lines represent NR recombination and radiative recombination, respectively, while the efficiencies are qualitatively depicted using line-thickness. In dry Ar (a), NR deep traps efficiently trap the carriers resulting in low emissivity from the band-edge ($h\nu_1$). In dry O_2 (b) or in H_2O (c), NR defects are passivated, while alternate shallow trap-mediated efficient emissive channels ($h\nu_2$ and $h\nu_3$) are operational. Generation of shallow NR traps due to photoexcitation in O_2/H_2O[10,11,31] likely leads to Mostly On blinking characteristics in these environments.

red shift (10−25 meV), indicating a reduced possibility of deep NR trap formation in moist air (as compared to Ar).

Subsequently, we investigated individual $MAPbBr_3$ NPs under varying moisture levels in Ar and in O_2 environments (without prior excitation in air) which allowed us to understand how water molecules in the surroundings interact with certain defects under photo illumination. As most emitters irreversibly degraded at high moistures (RH ∼ 60%), we were unable to collect statistical data on moisture dependent spectral characteristics. For few of these NPs which did survive prolonged moisture exposure, such as NP-6 (in Ar) and NP-7 (in O_2), we were able to quantify the changes in spectral features under varied moisture contents as shown in Figure 4. For NP-6, we find that the introduction of moisture in Ar leads to enormous (>100 times) intensity enhancement, along with ∼12−20 meV red shift in the transition energy (Figure 4a,b and Figure S12). These results illustrate that although Ar and light introduce deep NR traps, interaction of the NPs with moisture (in Ar) assists carriers to recombine via shallower radiative traps. We noticed that I_{PL} of NPs decreases dramatically within minutes of exposure to RH ∼ 60%, and most NPs are undetectable at higher RH. Interestingly, upon removal of moisture by purging dry Ar, both E_{PL} and I_{PL} of several NPs are found to revert back to that obtained initially in Ar (Figure 4b and Figure S12). This demonstrates the reversibility of formation/annihilation of radiative traps induced by physisorption of H_2O, for limited exposure up to certain amount of moisture (RH of 50%). Thus, exposure to low moisture in inert environments increases I_{PL}, while higher moisture (RH > 60%) most often irreversibly degrades $MAPbBr_3$ NPs.

The situation slightly changes for increasing moisture in oxygen environments. Figure 4c,d (also see Figure S13) shows the spectral characteristics of a representative NP in dry O_2 with increasing moisture, without prior illumination in air. As compared to O_2, NP-7 undergoes a 10-fold enhancement of I_{PL} in low moisture (RH ∼ 40%) along with a blue shift of ∼15−25 meV. However, further increase of moisture leads to decrease in I_{PL} close to that in O_2, while E_{PL} remains unchanged. This indicates shallow trap mediated RR is initiated by interaction of water molecules with the NPs even in the presence of high vapor pressure of oxygen. Therefore, we speculate that shallow trap-assisted emission in air (Figure 3a,b) owes to the moisture present in air, whereas our data indicated neat O_2 initiates RR from relatively deeper trap levels. We note that prolonged exposure to RH of 50% or beyond leads to complete quenching of PL for the vast majority of NPs (Figure S13), and we were unable to collect emission spectra even after removal of moisture in the environment by purging dry O_2 for 30 min. This suggests moist oxygen environment severely augments material degradation as well as optical instability of $MAPbBr_3$ NPs.

Origins of Environment-Induced Optical Instability of OHP NPs. Depending on certain specific interactions with atmospheric constituents in the presence of light, there can be variations in the optoelectronic behaviors among different NPs which remain obscured in ensemble measurements on TFs.[10,27,31,63] In agreement with previous reports,[33,42,63] we attribute significant quenching in I_{PL} under inert environment to the NR defects in the OHP NCs because of photoassisted ion mobility, which induces formation of deep midband energy states. Long-lived trapping of carriers in such NR defect states in dry Ar atmosphere renders low emission intensity via band edge, along with Mostly Off intermittency characteristics (Figure 5a). Under O_2/H_2O-free surroundings, most of the NPs are likely to remain chemically unchanged over illumination time scales, and thus qTSB behaviors are prevalent without severe photobleaching or photocuring effects. Emission intensity of majority of the NPs exhibits significantly enhanced I_{PL} along with Mostly On type blinking in the presence of electron coordinating atmospheric constituents such as O_2/H_2O molecules, which are known to passivate NR defects.[14,24,33,35] However, prolonged exposure to O_2 and/or H_2O in the presence of light severely degrades the $MAPbBr_3$ NPs rendering progressive rise in defect density, a hallmark of which is optical instability along with progressive decrease in the PL intensity. Further, considerable occurrence of BBB type intermittency in dry/moist aerobic conditions suggests that environmental activation and passivation of certain traps can be simultaneously operational which severely influence emissivity of individual emitters.

Our single-particle spectroscopic measurements on $MAPbBr_3$ NPs show that nature of the trap-mediated emission is selective toward different environmental constituents which has rarely been explored via theoretical[27] and experimental[10,55] investigations on OHP TFs. Enormous enhancement in I_{PL} along with large (∼80 meV) red shift of average E_{PL} in dry O_2 with respect to dry Ar indicates that oxygen passivates deep NR defects formed in Ar, while carriers are preferentially channelized through alternate traps where RR is facilitated

https://doi.org/10.1021/acs.jpcc.1c02207
J. Phys. Chem. C XXXX, XXX, XXX−XXX

(Figure 5b). A very similar process is likely operational in the presence of moisture (in Ar), albeit a lower red shift (~15−20 meV) in E_{PL} suggests efficient recombination through relatively shallow trap-assisted radiative channels (Figure 5c). Perhaps, interaction of oxygen/moisture with NPs leads to transient weakly bound species[27] or a negatively charged layer,[31] which removes certain NR traps[14,24,33,35] while creating few highly radiative traps,[10,55] thereby playing a major role to determine the nature of PL intermittency.

Despite similar effects based on the time scales of photobleaching, we find that interaction of $MAPbBr_3$ NPs with water vapor is more pronounced as compared to even neat oxygen. This likely is because of the larger scope of hydrogen bonding in H_2O as compared to molecular oxygen. Our spectral measurements under Ar(dry)−Ar(moist)−Ar-(dry) alternating environments show that the adverse effects of water as well as nature of traps involved in the emission process can often be reversed to a certain extent. We relate this phenomenon with low crystallinity as well as formation of hydrated $MAPbBr_3$ crystals at higher humidity level, consistent with recent *in situ* structural studies which show that crystallinity is (partially) restored when moisture content in the environment is lowered.[65] Thus, optical quality of OHP NPs and reversibility in moisture interaction is likely dependent on the amount of adsorbed/desorbed H_2O molecules on the NP surface, while neat O_2 treatment always leads to irreversible degradation of these OHP NPs. We emphasize here that the effect of O_2 and/or H_2O on optical instability and reversibility of I_{PL} and E_{PL} can also vary among NPs in the ensemble, perhaps depending on initial defect density of individual crystals. We surmise that the density and nature of defects on the NP surface are determined by a combination of factors such as surface coverage of capping ligands and interacting gas molecules. Depending on their nature, certain traps in each platelet likely act as the seeding points for other photogenerated defects which can initiate material degradation.

SUMMARY AND PERSPECTIVE

This work shows that systematic investigation of temporal evolution of single particle PL spectra can be useful to understand optical instability characteristics as well as energetics of carrier recombination in OHPs. Here, we focused on the PL intermittency and spectral characteristics of individual $MAPbBr_3$ NPs under diverse environmental conditions to obtain insights on the nature of various trap induced carrier recombination processes. Our results unveil that at least three distinct nature of (non)emissive traps can exist in $MAPbBr_3$ NPs which can specifically be activated/deactivated according to defect generation or passivation, especially in the presence of certain environmental constituent (O_2/H_2O). Further, we report the possibility of simultaneously operational annihilation as well as generation of defects for few OHP crystal where the latter dominates with time, likely due to environment-induced material degradation. Our data is consistent with inferences made on bulk $MAPbBr_3$ TFs under neat O_2, and light;[31,32] however, our blinking data additionally points to the continuous generation of active NR traps. Importantly, defect-assisted carrier recombination can be reversible in terms of both transition energies and PL intensities under photoillumination in consecutive inert (dry Ar) and O_2/H_2O rich conditions, which indicates switching between RR and NR channels with sequential changes in the environment. We speculate that (ir)reversibility between radiative and nonradiative defect mediated emission likely depends on extent of adsorption or percolation of O_2/H_2O through the NP surface.

We propose that O_2 along with H_2O in the environment provides the most detrimental condition toward optical and material stability of OHPs, which is an important factor to consider while developing perovskite based optoelectronic devices (solar cells/LEDs). On the other hand, to minimize the effects of oxygen and moisture, introduction of inert gases around active materials may also have adverse effects on the optoelectronic properties because of the generation of nonradiative deep traps, which can significantly reduce the radiative efficiency and perhaps, hinder carrier transport as well. Hopefully, this work provides some clues to unambiguously decipher the nature of environmental interactions with OHPs as well as their degradation mechanisms.

ASSOCIATED CONTENT

Supporting Information

The Supporting Information is available free of charge at https://pubs.acs.org/doi/10.1021/acs.jpcc.1c02207.

Structural and electronic characterization of $MAPbBr_3$ NPs, PL intermittency characteristics, and spectral trajectories of more NPs under sequential environmental changes, along with statistics of spectral features on ~80 NPs are provided as Figures S1−13 and Table S1 (PDF)

AUTHOR INFORMATION

Corresponding Authors

Arindam Chowdhury − *Department of Chemistry, Indian Institute of Technology Bombay, Powai, Mumbai 400076, India*; orcid.org/0000-0001-8178-1061; Email: arindam@chem.iitb.ac.in

Mohammed Aslam − *Department of Physics, Indian Institute of Technology Bombay, Powai, Mumbai 400076, India*; Email: m.aslam@iitb.ac.in

Authors

Amitrajit Mukherjee − *Department of Chemistry, Indian Institute of Technology Bombay, Powai, Mumbai 400076, India*

Mrinmoy Roy − *Department of Physics, Indian Institute of Technology Bombay, Powai, Mumbai 400076, India*; orcid.org/0000-0002-6503-6405

Nithin Pathoor − *Department of Chemistry, Indian Institute of Technology Bombay, Powai, Mumbai 400076, India*

Complete contact information is available at: https://pubs.acs.org/10.1021/acs.jpcc.1c02207

Notes

The authors declare no competing financial interest.

ACKNOWLEDGMENTS

A.M. acknowledges NCPRE (IIT Bombay)-Phase II, through MNRE (Government of India), for funding scholarship, M.R. thanks IIT Bombay, MHRD for fellowship, A.M., M.A and A.C. gratefully acknowledge scholarship and financial support by MNRE (Government of India) supported NCPRE at IIT Bombay. A.C. acknowledges DST (Government of India) SERB Grant EMR/2017/004878 to carry out this work.

Authors acknowledge SAIF at IIT Bombay for usage of central facility equipment.

REFERENCES

(1) Green, M. A.; Ho-Baillie, A.; Snaith, H. J. The Emergence of Perovskite Solar Cells. *Nat. Photonics* **2014**, *8*, 506−514.

(2) Burschka, J.; Pellet, N.; Moon, S.-J.; Humphry-Baker, R.; Gao, P.; Nazeeruddin, M. K.; Gratzel, M. Sequential Deposition as a Route to High-performance Perovskite-sensitized Solar Cells. *Nature* **2013**, *499*, 316−319.

(3) Tan, Z.-K.; Moghaddam, R. S.; Lai, M. L.; Docampo, P.; Higler, R.; Deschler, F.; Price, M.; Sadhanala, A.; Pazos, L. M.; Credgington, D.; et al. Bright Light-emitting Diodes Based on Organometal Halide Perovskite. *Nat. Nanotechnol.* **2014**, *9*, 687−692.

(4) Xiao, Z.; Kerner, R. A.; Zhao, L.; Tran, N. L.; Lee, K. M.; Koh, T.-W.; Scholes, G. D.; Rand, B. P. Efficient Perovskite Light-emitting Diodes Featuring Nanometre-sized Crystallites. *Nat. Photonics* **2017**, *11*, 108−116.

(5) Chen, S.; Roh, K.; Lee, J.; Chong, W. K.; Lu, Y.; Mathews, N.; Sum, T. C.; Nurmikko, A. A Photonic Crystal Laser from Solution Based Organo-Lead Iodide Perovskite Thin Films. *ACS Nano* **2016**, *10*, 3959−3967.

(6) Sutherland, B. R.; Sargent, E. D. Perovskite Photonic Sources. *Nat. Photonics* **2016**, *10*, 295−302.

(7) Xing, G. C.; Mathews, N.; Sun, S. Y.; Lim, S. S.; Lam, Y. M.; Gratzel, M.; Mhaisalkar, S.; Sum, T. C.; et al. Long-Range Balanced Electron- and Hole-Transport Lengths in Organic-Inorganic $CH_3NH_3PbI_3$. *Science* **2013**, *342*, 344−347.

(8) Stranks, S. D.; Eperon, G. E.; Grancini, G.; Menelaou, C.; Alcocer, M. J. P.; Leijtens, T.; Herz, L. M.; Petrozza, A.; Snaith, H. J. Electron-Hole Diffusion Lengths Exceeding 1 Micrometer in an Organometal Trihalide Perovskite Absorber. *Science* **2013**, *342*, 341−344.

(9) Jin, H.; Debroye, E.; Keshavarz, M.; Scheblykin, I. G.; Roeffaers, M. B. J.; Hofkens, J.; Steele, J. A. It's a Trap! On the Nature of Localised States and Charge Trapping in Lead Halide Perovskites. *Mater. Horiz.* **2020**, *7*, 397−410.

(10) Segovia, R.; Qu, G.; Peng, M.; Sun, X.; Shi, H.; Gao, B.; et al. Evolution of Photoluminescence, Raman, and Structure of $CH_3NH_3PbI_3$ Perovskite Microwires Under Humidity Exposure. *Nanoscale Res. Lett.* **2018**, *13*, 79−86.

(11) Seth, C.; Khushalani, D. Degradation and Regeneration of Hybrid Perovskites. *RSC Adv.* **2016**, *6*, 101846−101852.

(12) Aristidou, N.; Sanchez-Molina, I.; Chotchuangchutchaval, T.; Brown, M.; Martinez, L.; Rath, T.; Haque, S. A. The Role of Oxygen in the Degradation of Methylammonium Lead Trihalide Perovskite Photoactive Layers. *Angew. Chem., Int. Ed.* **2015**, *54*, 8208−8212.

(13) Aristidou, N.; Eames, C.; Sanchez-Molina, I.; Bu, X.; Kosco, J.; Islam, M. S.; Haque, S. A. Fast Oxygen Diffusion and Iodide Defects Mediate Oxygen-induced Degradation of Perovskite Solar Cells. *Nat. Commun.* **2017**, *8*, 15218.

(14) Chouhan, L.; Ghimire, S.; Biju, V. Blinking Beats Bleaching: The Control of Superoxide Generation by Photo-ionized Perovskite Nanocrystals. *Angew. Chem.* **2019**, *131*, 4929−4933.

(15) Yang, J.; Yuan, Z.; Liu, X.; Braun, S.; Li, Y.; Tang, J.; Gao, F.; Duan, C.; Fahlman, M.; Bao, Q. Oxygen- and Water-Induced Energetics Degradation in Organometal Halide Perovskites. *ACS Appl. Mater. Interfaces* **2018**, *10*, 16225−16230.

(16) Zheng, C.; Rubel, O.; et al. Unraveling the Water Degradation Mechanism of $CH_3NH_3PbI_3$. *J. Phys. Chem. C* **2019**, *123*, 19385−19394.

(17) Strachala, D.; Kratochvil, M.; Hylsky, J.; Gajdos, A.; Cudek, P.; Vanek, J. Perovskite Solar Cells with Increased Resistance to Moisture. *ECS Trans.* **2018**, *87*, 199.

(18) Idígoras, J.; Aparicio, F. J.; Contreras-Bernal, L.; Ramos-Terrón, S.; Alcaire, M.; Sánchez-Valenciá, J. R.; Borras, A.; Barranco, Á.; Anta, J. A. Enhancing Moisture and Water Resistance in Perovskite Solar Cells by Encapsulation with Ultrathin Plasma Polymers. *ACS Appl. Mater. Interfaces* **2018**, *10*, 11587−11594.

(19) Boyd, C. C.; Cheacharoen, R.; Leijtens, T.; McGehee, M. D. Understanding Degradation Mechanisms and Improving Stability of Perovskite Photovoltaics. *Chem. Rev.* **2019**, *119*, 3418−3451.

(20) Tong, C.-J.; Geng, W.; Tang, Z.-K.; Yam, C.-Y.; Fan, X.-L.; Liu, J.; Lau, W.-M.; Liu, L.-M.; et al. Uncovering the Veil of the Degradation in Perovskite $CH_3NH_3PbI_3$ upon Humidity Exposure: A First-Principles Study. *J. Phys. Chem. Lett.* **2015**, *6*, 3289−3295.

(21) Christians, J. A.; Miranda Herrera, P. A.; Kamat, P. V.; et al. Transformation of the Excited State and Photovoltaic Efficiency of $CH_3NH_3PbI_3$ Perovskite upon Controlled Exposure to Humidified Air. *J. Am. Chem. Soc.* **2015**, *137*, 1530−1538.

(22) Yang, J.; Siempelkamp, B. D.; Liu, D.; Kelly, T. L.; et al. Investigation of $CH_3NH_3PbI_3$ Degradation Rates and Mechanisms in Controlled Humidity Environments Using *in Situ* Techniques. *ACS Nano* **2015**, *9*, 1955−1963.

(23) Kwak, K.; Lim, E.; Ahn, N.; Heo, J.; Bang, K.; Kim, S. K.; Choi, M. An Atomistic Mechanism for the Degradation of Perovskite Solar Cells by Trapped Charge. *Nanoscale* **2019**, *11*, 11369−11378.

(24) Tian, Y.; Peter, M.; Unger, E.; Abdellah, M.; Zheng, K.; Pullerits, T.; Yartsev, A.; Sundstrom, V.; Scheblykin, I. G. Mechanistic Insights into Perovskite Photoluminescence Enhancement: Light Curing with Oxygen can Boost Yield Thousandfold. *Phys. Chem. Chem. Phys.* **2015**, *17*, 24978−24987.

(25) Tian, Y.; Merdasa, A.; Unger, E.; Abdellah, M.; Zheng, K.; McKibbin, S.; Mikkelsen, A.; Pullerits, T.; Yartsev, A.; Sundström, V.; et al. Enhanced Organo-Metal Halide Perovskite Photoluminescence from Nanosized Defect-Free Crystallites and Emitting Sites. *J. Phys. Chem. Lett.* **2015**, *6*, 4171−4177.

(26) Brenes, R.; Eames, C.; Bulović, V.; Islam, M. S.; Stranks, S. D. The Impact of Atmosphere on the Local Luminescence Properties of Metal Halide Perovskite Grains. *Adv. Mater.* **2018**, *30*, 1706208.

(27) Meggiolaro, D.; Mosconi, E.; De Angelis, F. Mechanism of Reversible Trap Passivation by Molecular Oxygen in Lead-Halide Perovskites. *ACS Energy Lett.* **2017**, *2*, 2794−2798.

(28) Fang, H.-H.; Adjokatse, S.; Wei, H.; Yang, J.; Blake, G. R.; Huang, J.; Even, J.; Loi, M. A. Ultrahigh Sensitivity of Methylammonium Lead Tribromide Perovskite Single Crystals to Environmental Gases. *Sci. Adv.* **2016**, *2*, No. e1600534.

(29) Eperon, G. E.; Habisreutinger, S. N.; Leijtens, T.; Bruijnaers, B. J.; van Franeker, J. J.; deQuilettes, D. W.; Pathak, S.; Sutton, R. J.; Grancini, G.; Ginger, D. S.; et al. The Importance of Moisture in Hybrid Lead Halide Perovskite Thin Film Fabrication. *ACS Nano* **2015**, *9*, 9380−9393.

(30) Halder, A.; Pathoor, N.; Chowdhury, A.; Sarkar, S. K. Photoluminescence Flickering of Micron-Sized Crystals of Methylammonium Lead Bromide: Effect of Ambience and Light Exposure. *J. Phys. Chem. C* **2018**, *122*, 15133−15139.

(31) Anaya, M.; Galisteo-Lopez, J. F.; Calvo, M. E.; Espinos, J. P.; Míguez, H. Origin of Light-Induced Photophysical Effects in Organic Metal Halide Perovskites in the Presence of Oxygen. *J. Phys. Chem. Lett.* **2018**, *9*, 3891−3896.

(32) van de Riet, I.; Fang, H.-H.; Adjokatse, S.; Kahmann, S.; Loi, M. A. Influence of morphology on photoluminescence properties of methylammonium lead tribromide films. *J. Lumin.* **2020**, *220*, 117033.

(33) Galisteo-López, J. F.; Calvo, M. E.; Rojas, T. C.; Míguez, H. Mechanism of Photoluminescence Intermittency in Organic-Inorganic Perovskite Nanocrystals. *ACS Appl. Mater. Interfaces* **2019**, *11*, 6344−6349.

(34) Wen, X.; Ho-Baillie, A.; Huang, S.; Sheng, R.; Chen, S.; Ko, H.-C.; Green, M. A. Mobile Charge-Induced Fluorescence Intermittency in Methylammonium Lead Bromide Perovskite. *Nano Lett.* **2015**, *15*, 4644−4649.

(35) Vicente, J. R.; Rafiei Miandashti, A.; Sy Piecco, K. W. E.; Pyle, J. R.; Kordesch, M. E.; Chen, J. Single-Particle Organolead Halide Perovskite Photoluminescence as a Probe for Surface Reaction Kinetics. *ACS Appl. Mater. Interfaces* **2019**, *11*, 18034−18043.

(36) Merdasa, A.; Tian, Y.; Camacho, R.; Dobrovolsky, A.; Debroye, E.; Unger, E. L.; Hofkens, J.; Sundström, V.; Scheblykin, I. G. Supertrap" at Work: Extremely Efficient Nonradiative Recombination

https://doi.org/10.1021/acs.jpcc.1c02207
J. Phys. Chem. C XXXX, XXX, XXX−XXX

Channels in $MAPbI_3$ Perovskites Revealed by Luminescence Super-Resolution Imaging and Spectroscopy. *ACS Nano* **2017**, *11*, 5391−5404.
(37) Behera, T.; Pathoor, N.; Phadnis, C.; Buragohain, S.; Chowdhury, A. Spatially Correlated Photoluminescence Blinking and Flickering of Hybrid-halide Perovskite Micro-rods. *J. Lumin.* **2020**, *223*, 117202.
(38) Tian, Y.; Merdasa, A.; Peter, M.; Abdellah, M.; Zheng, K.; Ponseca, C. S., Jr.; Pullerits, T.; Yartsev, A.; Sundström, V.; Scheblykin, I. G. Giant Photoluminescence Blinking of Perovskite Nanocrystals Reveals Single-trap Control of Luminescence. *Nano Lett.* **2015**, *15*, 1603−1608.
(39) Zhu, F.; Men, L.; Guo, Y.; Zhu, Q.; Bhattacharjee, U.; Goodwin, P. M.; Petrich, J. W.; Smith, E. A.; Vela, J. Shape Evolution and Single Particle Luminescence of Organometal Halide Perovskite Nanocrystals. *ACS Nano* **2015**, *9*, 2948−2959.
(40) Pathoor, N.; Halder, A.; Mukherjee, A.; Mahato, J.; Sarkar, S. K.; Chowdhury, A. Fluorescence Blinking Beyond Nanoconfinement: Spatially Synchronous Intermittency of Entire Perovskite Microcrystals. *Angew. Chem., Int. Ed.* **2018**, *57*, 11603−11607.
(41) Frantsuzov, P. A.; Kuno, M.; Janko, B.; Marcus, R. A. Universal Emission Intermittency in Quantum Dots, Nanorods and Nanowires. *Nat. Phys.* **2008**, *4*, 519−522.
(42) Motti, S. G.; Gandini, M.; Barker, A. J.; Ball, J. M.; Srimath Kandada, A. R.; Petrozza, A. Photoinduced Emissive Trap States in Lead Halide Perovskite Semiconductors. *ACS Energy Lett.* **2016**, *1*, 726−730.
(43) Kim, G. Y.; Senocrate, A.; Yang, T.-Y.; Gregori, G.; Grätzel, M.; Maier, J. Large Tunable Photoeffect on Ion Conduction in Halide Perovskites and Implications for Photodecomposition. *Nat. Mater.* **2018**, *17*, 445−449.
(44) Mosconi, E.; Meggiolaro, D.; Snaith, H. J.; Stranks, S. D.; De Angelis, F. Light-induced Annihilation of Frenkel Defects in Organo-lead Halide Perovskites. *Energy Environ. Sci.* **2016**, *9*, 3180−3187.
(45) Yuan, G.; Ritchie, C.; Ritter, M.; Murphy, S.; Gómez, D. E.; Mulvaney, P. The Degradation and Blinking of Single $CsPbI_3$ Perovskite Quantum Dots. *J. Phys. Chem. C* **2018**, *122*, 13407−13415.
(46) Park, Y.-S.; Guo, S.; Makarov, N. S.; Klimov, V. I. Room Temperature Single-Photon Emission from Individual Perovskite Quantum Dots. *ACS Nano* **2015**, *9*, 10386−10393.
(47) Swarnkar, A.; Chulliyil, R.; Ravi, V. K.; Irfanullah, M.; Chowdhury, A.; Nag, A. Colloidal $CsPbBr_3$ Perovskite Nanocrystals: Luminescence Beyond Traditional Quantum Dots. *Angew. Chem., Int. Ed.* **2015**, *54*, 15424−15428.
(48) Mukherjee, A.; Ray, K. K.; Phadnis, C.; Layek, A.; Bera, S.; Chowdhury, A. Insights on Heterogeneity in Blinking Mechanisms and Non-ergodicity Using Sub-ensemble Statistical Analysis of Single Quantum-dots. *J. Chem. Phys.* **2019**, *151*, 084701.
(49) Yuan, H.; Debroye, E.; Bladt, E.; Lu, G.; Keshavarz, M.; Janssen, K. P. F.; Roeffaers, M. B. J.; Bals, S.; Sargent, E. H.; Hofkens, J. Imaging Heterogeneously Distributed Photo-Active Traps in Perovskite Single Crystals. *Adv. Mater.* **2018**, *30*, 1705494.
(50) Hong, D.; Zhou, Y.; Wan, S.; Hu, X.; Xie, D.; Tian, Y. Nature of Photoinduced Quenching Traps in Methylammonium Lead Triiodide Perovskite Revealed by Reversible Photoluminescence Decline. *ACS Photonics* **2018**, *5*, 2034−2043.
(51) DeQuilettes, D. W.; Vorpahl, S. M.; Stranks, S. D.; Nagaoka, H.; Eperon, G. E.; Ziffer, M. E.; Snaith, H. J.; Ginger, D. S. Impact of Microstructure on Local Carrier Lifetime in Perovskite Solar Cells. *Science* **2015**, *348*, 683−686.
(52) Brennan, M. C.; Draguta, S.; Kamat, P. V.; Kuno, M. Light-Induced Anion Phase Segregation in Mixed Halide Perovskites. *ACS Energy Lett.* **2018**, *3*, 204−213.
(53) Halder, A.; Chulliyil, R.; Subbiah, A. S.; Khan, T.; Chattoraj, S.; Chowdhury, A.; Sarkar, S. K. Pseudohalide (SCN^-)-Doped $MAPbI_3$ Perovskites: A Few Surprises. *J. Phys. Chem. Lett.* **2015**, *6*, 3483−3489.
(54) Duim, H.; Fang, H.-H.; Adjokatse, S.; ten Brink, G. H.; Marques, M. A. L.; Kooi, B. J.; Blake, G. R.; Botti, S.; Loi, M. A. Mechanism of Surface Passivation of Methylammonium Lead Tribromide Single Crystals by Benzylamine. *Appl. Phys. Rev.* **2019**, *6*, 031401.
(55) Ghosh, S.; Pal, S. K.; Karki, K. J.; Pullerits, T. Ion Migration Heals Trapping Centers in $CH_3NH_3PbBr_3$ Perovskite. *ACS Energy Lett.* **2017**, *2*, 2133−2139.
(56) Gerhard, M.; Louis, B.; Frantsuzov, P. A.; Li, J.; Kiligaridis, A.; Hofkens, J.; Scheblykin, I. G. Heterogeneities and Emissive Defects in $MAPbI_3$ Perovskite Revealed by Spectrally Resolved Luminescence Blinking. *Adv. Opt. Mater.* **2021**, 2001380.
(57) Ling, Y.; Yuan, Z.; Tian, Y.; Wang, X.; Wang, J. C.; Xin, Y.; Hanson, K.; Ma, B.; Gao, H. Bright Light-Emitting Diodes Based on Organometal Halide Perovskite Nanoplatelets. *Adv. Mater.* **2016**, *28*, 305−311.
(58) Wang, S.-P.; Chang, C.-K.; Yang, S.-H.; Chang, C.-Y.; Chao, Y.-C. Novel Hybrid Light-Emitting Devices Based on $MAPbBr_3$ Nanoplatelets: PVK Nanocomposites and Zinc Oxide Nanorod Arrays. *Mater. Res. Express* **2018**, *5*, 015037.
(59) Li, R.; Xu, Y.; Li, W.; Li, Y.; Peng, J.; Xu, M.; Lin, Q. Layered Perovskites Enhanced Perovskite Photodiodes. *J. Phys. Chem. Lett.* **2021**, *12*, 1726−1733.
(60) Roy, M.; Vikram Banerjee, S.; Mitra, A.; Alam, A.; Aslam, M. Composition-Controlled Synthesis of Hybrid Perovskite Nanoparticles by Ionic Metathesis: Bandgap Engineering Studies from Experiments and Theoretical Calculations. *Chem. - Eur. J.* **2019**, *25*, 9892−9901.
(61) Tauc, J. Optical properties and electronic structure of amorphous Ge and Si. *Mater. Res. Bull.* **1968**, *3*, 37−46.
(62) Hazarika, A.; Layek, A.; De, S.; Nag, A.; Debnath, S.; Mahadevan, P.; Chowdhury, A.; Sarma, D. D. Ultranarrow and Widely Tunable Mn^{2+}-Induced Photoluminescence from Single Mn-Doped Nanocrystals of ZnS-CdS Alloys. *Phys. Rev. Lett.* **2013**, *110*, 26740.
(63) Galisteo-López, J. F.; Anaya, M.; Calvo, M. E.; Míguez, H. Environmental Effects on the Photophysics of Organic−Inorganic Halide Perovskites. *J. Phys. Chem. Lett.* **2015**, *6*, 2200−2205.
(64) Lorenzon, M.; Sortino, L.; Akkerman, Q.; Accornero, S.; Pedrini, J.; Prato, M.; Pinchetti, V.; Meinardi, F.; Manna, L.; Brovelli, S. Role of Nonradiative Defects and Environmental Oxygen on Exciton Recombination Processes in $CsPbBr_3$ Perovskite Nanocrystals. *Nano Lett.* **2017**, *17*, 3844−3853.
(65) Girolamo, D. D.; Dar, M. I.; Dini, D.; Gontrani, L.; Caminiti, R.; Mattoni, A.; Graetzel, M.; Meloni, S. Dual Effect of Humidity on Cesium Lead Bromide: Enhancement and Degradation of Perovskite Films. *J. Mater. Chem. A* **2019**, *7*, 12292.

https://doi.org/10.1021/acs.jpcc.1c02207
J. Phys. Chem. C XXXX, XXX, XXX−XXX